Direct numerical simulation of a self-similar adverse pressure gradient turbulent boundary layer

V. Kitsios[a,*], C. Atkinson[a], J.A. Sillero[b], G. Borrell[b], A. G. Gungor[c], J. Jiménez[b], J. Soria[a,d]

[a] *Laboratory For Turbulence Research in Aerospace and Combustion, Department of Mechanical and Aerospace Engineering, Monash University, Clayton 3800, AUSTRALIA*
[b] *School of Aeronautics, Universidad Politécnica de Madrid, E-28040 Madrid, SPAIN*
[c] *Istanbul Technical University, Department of Astronautical Engineering, Maslak 34469 Istanbul, TURKEY*
[d] *Department of Aeronautical Engineering, King Abdulaziz University, Jeddah 21589, KINGDOM OF SAUDI ARABIA*

Abstract

The statistical properties of a self-similar adverse pressure gradient (APG) turbulent boundary layer (TBL) are presented. The flow is generated via the direct numerical simulation (DNS) of a TBL on a flat surface with a farfield boundary condition designed to apply the desired pressure gradient. The conditions for self-similarity and appropriate scaling are derived, with the mean profiles, Reynolds stress profiles, and turbulent kinetic energy budgets non-dimensionalised using this scaling. The APG TBL has a momentum thickness based Reynolds number range from $Re_{\delta_2} = 300$ to 6000, with a self-similar region spanning a Reynolds number range from $Re_{\delta_2} = 3500$ to 4800. Within this range the non-dimensional pressure gradient parameter $\beta = 1$. Two-point correlations of each of the velocity components in the streamwise/wall-normal plane are also presented, which illustrate the statistical imprint of the structures in this plane for the APG TBL.

Keywords: Direct Numerical Simulation, Adverse Pressure Gradient, Turbulent Boundary Layer

*Corresponding author
Email address: vassili.kitsios@monash.edu (V. Kitsios)

1. Introduction

The efficient design and performance of many engineering systems rely on fluid flows remaining attached to aerodynamic surfaces in regions of adverse pressure gradient (APG). Separation of the boundary layer can potentially result in catastrophic consequences or at best sub-optimal performance. Adverse pressure gradients typically arise due to the presence of convex curved surfaces, such as those on wind turbine blades, turbo-machinery and aircraft wings. These configurations are difficult to systematically study, since the pressure gradient applied to the turbulent boundary layer (TBL) is constantly changing in the streamwise direction [1]. There has been a long history of theoretical, experimental and numerical research into TBL. The vast majority of the research, however, has been centred on the zero pressure gradient (ZPG) case, while many aspects of turbulent structure and appropriate scaling of APG TBL remain largely unresolved. The study of APG turbulent boundary layers (TBL) in an appropriate canonical form is, therefore, of utmost importance to understand the influence of local pressure gradient.

The most appropriate canonical APG TBL to study is arguably one that is self-similar. A self-similar TBL (or portion thereof) is defined as one in which each of the terms in the governing equations have the same proportionality with streamwise position over the domain of interest [2, 3, 4]. According to the definition in [3], this means that the non-dimensional pressure gradient, $\beta = \delta_1(\partial_x P_e)/\tau_w$, must be constant, where $\partial_x P_e$ is the farfield pressure gradient, δ_1 is the displacement thickness, and τ_w is the mean shear stress at the well. Note this definition will be broadened in section 3 of the present manuscript. For a ZPG TBL $\beta = 0$, for a favorable pressure gradient (FPG) $\beta < 0$, for an APG $\beta > 0$, and immediately prior to separation $\beta \to \infty$. Imagine two boundary layers, one starting with an APG that is then accelerated to ZPG, and another starting with a FPG that is then decelerated to ZPG. The statistical properties at the position of ZPG of these two scenarios are different from each other, and also different from the canonical ZPG flow [5]. The flow structure, statistics,

stability properties and scaling are all dependent upon the specific streamwise distribution of the pressure gradient. This illustrates the challenge of APG TBL studies and the value of studying the self-similar case.

Much of the theoretical work in the study of APG TBL is based on deriving the conditions and scaling properties for self-similar boundary layers, in which all statistics collapse down onto a single set of profiles for a given pressure gradient [2, 6, 3, 7, 8, 4, 9, 10, 11]. Additional theoretical studies have focussed specifically on the limiting case of zero-shear-stress ($\beta \to \infty$) self-similar APG TBL, which is the scenario immediately prior to the point of mean separation [12, 13]. Attempts have also been made to collapse the statistical profiles of non-self-similar APG TBL using various definitions of the pertinent velocity and length scales [14, 15, 16].

There have been numerous experimental campaigns studying the effect of APG. Most of these studies have focussed on the statistical velocity profiles [17, 18, 19, 20, 21], with some recent measurements also presenting information on the spatial structure of such flows [22]. A smaller number of experiments have also attempted to produce self-similar boundary layers, in which the statistical profiles at various streamwise positions collapse under the appropriate scaling [23, 24, 25]. The study of [24] in particular focussed on the $\beta \to \infty$ case with a momentum thickness based Reynolds number, $Re_{\delta_2} = 4 \times 10^4$. The consistent observation across all of these studies, is the presence of a second outer peak in the variance of the velocity fluctuations located further away from the wall than the inner peak observed in ZPG TBL. This is due to the shear being distributed throughout the boundary layer imparted by the pressure gradient. This outer peak also becomes more prominent with increasing pressure gradient.

DNS have also been undertaken of both self-similar and non-self-similar APG TBL. Each of the following DNS are performed in a rectangular domain, with the APG applied via the prescription of the farfield boundary condition. The first DNS of an APG TBL was that of the [26], which produced a non-self-similar TBL with $Re_{\delta_2} = 1600$, and $\beta = 2$. There have also been several DNS of separated APG flows [27, 28, 29], with the most recent of which [29] having

the largest Reynolds number of $Re_{\delta_2} = 2175$. The only attempted DNS of self-similar boundary layers are those of [30] and [31]. In the study of [30] two DNS were presented, the first with Reynolds numbers ranging from $Re_{\delta_2} = 390$ to 620 with $\beta = 0.24$, and the second having a Reynolds number range of $Re_{\delta_2} = 430$ to 690 with $\beta = 0.65$. In the more recent study of [31] a higher Reynolds number APG TBL DNS was presented with $Re_{\delta_2} = 1200$ to 1400, and also with a stronger pressure gradient of $\beta = 1.68$.

The focus of the present study is to add to the current body of APG TBL DNS databases, and in particular address the need for higher Reynolds number self-similar APG flows. Specifically we present a DNS of an APG TBL with a Reynolds number range of $Re_{\delta_2} = 300$ to 6000, which is larger in both range and magnitude of the aforementioned APG TBL DNS studies. Self-similarity of the TBL is also demonstrated from $Re_{\delta_2} = 3500$ to 4800, within which $\beta = 1$. In the current manuscript we present the details of DNS, characterise the APG TBL on the basis of scaling properties, one-point and two-point statistics. Firstly in section 2, an overview of the TBL DNS code is presented along with the farfield boundary condition (BC) required to generate the self-similar APG TBL. The APG TBL is characterised and compared to the ZPG TBL on the basis of standard boundary layer properties including integral length and velocity scales. In section 3, the conditions for self-similarity (and associated scaling) are derived from the boundary layer equations and evaluated for both the APG and ZPG cases. Profiles of the mean velocity deficit and Reynolds stresses from the DNS of the APG are then compared to those of the ZPG DNS on the basis of both the derived scaling and also viscous scaling in section 4. In section 5 two-point correlations of each of the velocity components are presented in the streamwise/wall-normal plane for the APG TBL and contrasted with previous ZPG DNS results. Finally concluding remarks are made in section 6.

2. Direct numerical simulation

The code adopted within solves the Navier-Stokes equations in a three-dimensional rectangular volume, with constant density (ρ) and kinematic viscosity (ν). The three flow directions are the streamwise (x), wall-normal (y) and spanwise (z), with instantaneous velocity components in these directions of U, V and W. Notation used for the derivative operators in these directions are $\partial_x \equiv \partial/\partial x$, $\partial_y \equiv \partial/\partial y$, and $\partial_z \equiv \partial/\partial z$. Throughout the paper the mean velocity components are represented by $(\langle U\rangle, \langle V\rangle, \langle W\rangle)$, with the averaging undertaken both in time and along the spanwise direction. The associated fluctuating velocity components are (u, v, w).

Details of the algorithmic approach to solve the equations of motion are as follows. A fractional-step method is used to solve the governing equations for the velocity and pressure (P) fields [32, 33]. Fourier decomposition is used in the periodic spanwise direction, with compact finite difference in the aperiodic wall-normal and streamwise directions [34]. The equations are stepped forward in time using a modified three sub-step Runge-Kutta scheme [35]. The code utilises MPI and openMP parallelisation to decompose the domain. For further details on the code and parallelisation, the interested reader should refer to [36, 37]. In the following sections we present: the boundary conditions necessary to implement the ZPG and APG TBL; numerical details; and characterise both the APG and ZPG TBL flows.

2.1. Boundary conditions

The boundary conditions of the ZPG TBL DNS code are outlined below. The bottom surface is a flat plate with a no-slip (zero velocity) BC. The spanwise boundaries are periodic. Due to the TBL growing in height as it develops in the streamwise direction, a downstream streamwise normal recycling plane is copied, and mapped to the inlet BC [38]. At the farfield boundary a zero spanwise vorticity condition is applied, and the wall normal velocity specified. It is important that the wall normal velocity be prescribed, as opposed to the

streamwise velocity, so as to not over constrain the system [39]. This may not be a significant problem for ZPG TBL, but becomes an increasingly significant issue as the pressure gradient increases. The wall normal velocity at this boundary is given by

$$V_{ZPG}(x) \quad = \quad U_{ZPG}\ \partial_x \delta_1(x)\ , \tag{1}$$

where U_{ZPG} is the constant freestream streamwise velocity, and δ_1 is the displacement thickness [37].

Due to the properties of the APG TBL, we also use a slightly different definition of displacement (δ_1) thickness, and of the momentum thickness (δ_2) for that matter. These length scales are given by

$$\delta_1(x) \quad = \quad \int_0^{\delta(x)} \left(1 - \frac{\langle U \rangle(x,y)}{U_e(x)}\right)\ dy\ \text{, and} \tag{2}$$

$$\delta_2(x) \quad = \quad \int_0^{\delta(x)} \left(1 - \frac{\langle U \rangle(x,y)}{U_e(x)}\right) \frac{\langle U \rangle(x,y)}{U_e(x)}\ dy\ , \tag{3}$$

where $\delta(x)$ is the wall normal position of the maximum velocity along the profile, $U_e(x)$. We require this modified definition, because at the farfield boundary of the APG TBL $\partial V_\infty / \partial x$ is not necessarily negligible, and less than zero. This means for the farfield to have zero spanwise vorticity, $\partial U_\infty / \partial y$ must also be less than zero. The $\langle U \rangle$ profile, therefore, has a turning point in y. The integrals in (2) and (3) must then stop at this turning point ($y = \delta(x)$).

To generate the self-similar APG TBL flow, the farfield wall-normal velocity BC must be derived. The wall normal suction velocity $V_{APG}(x)$ is deduced from $U_{APG}(x)$ via the boundary layer streamfunction solution [3] in the farfield region as

$$V_{APG}(x) = -\left[y_\infty - \delta_1(x)\right]\ \partial_x U_{APG}(x) + U_{APG}(x)\ \partial_x \delta_1(x)\ , \tag{4}$$

where y_∞ is the wall normal position of the farfield boundary. To implement such a boundary condition in the DNS, we use the specific values for the incipient separation case from [3], where the freestream streamwise velocity $U_{APG}(x)/U_\infty(x_0) = (x - x_{\text{origin}})^{-0.23}$, and $\delta_1(x) = 0.041(x - x_{\text{origin}})$, where

x_{origin} is the virtual origin of the boundary layer, which in the present DNS is set to $x_{\text{origin}} = x_s$. Equation (4) can also be deduced from the similarity analysis of continuity equation section 3.

The structure of the complete farfield wall normal BC, $V_\infty(x)$, is as follows. In the APG TBL DNS, to allow the rescaling necessary for the inlet BC, an initial ZPG TBL is simulated up until the streamwise position $x_s = 500\delta_1(x_0)$ (located after the recycling plane) by applying $V_{ZPG}(x)$ as defined in (1). Note $\delta_1(x_0)$ is the displacement thickness at the inlet of position $x = x_0$. Downstream of the position $x_f = 700\delta_1(x_0)$ the wall normal velocity $V_{APG}(x)$ is applied at the farfield boundary as given by (4), which imparts the desired deceleration and hence, expansion of the boundary layer. From x_s to x_f the velocity $V_{APG}(x)$ is gradually introduced using a smoothing function. Finally the farfield velocity is transitioned from suction ($V_\infty(x) > 0$) at $x_b = 3800\delta_1(x_0)$ to blowing ($V_\infty(x) < 0$) at the outlet to reduce the number of instantaneous reversed flow events, to ensure that numerical stability of the outflow BC is maintained. The ZPG and APG farfield boundary conditions, $V_\infty(x)/U_\infty(x_0)$, are illustrated in Fig. 1, where $U_\infty(x_0)$ is the freestream streamwise velocity at the inlet.

2.2. Numerical details

The numerical details of the ZPG and APG simulations are summarised in table 1. The number of grid points in the streamwise, wall normal and spanwise directions are given by N_x,N_y, and N_z, respectively, along with the extents of the computational domain in these directions (L_x, L_y, L_z). The computational domain size is first non-dimensionalised with respect to the inlet boundary layer thickness ($\delta_{99}(x_0)$), which is the same in both the APG and ZPG simulations. Since the APG profiles of $\langle U \rangle$ have a turning point in y, $\delta_{99}(x)$ is defined as the smallest value of y for which $\langle U \rangle(x, y) = 0.99\, U_e(x)$. The APG case has a larger wall normal domain (L_y) and more points in this direction (N_y), which is necessary since the APG TBL expands more quickly while evolving in the streamwise direction than the ZPG TBL. In fact with respect to the boundary layer thickness ($\delta_{99}(x_m)$) at the centre of the domain of interest ($x_m = 2500\delta_1(x_0)$), the

APG case has a larger wall normal domain of $L_y = 4.72\delta_{99}(x_m)$, as opposed to $L_y = 3.80\delta_{99}(x_m)$ for the ZPG case.

The grid resolutions are also presented in table 1. The grid spacings in the streamwise (Δx) and spanwise directions (Δz) are constant. The smallest wall normal grid spacing is located at the wall (Δy_{wall}), and increases monotonically to the maximum wall normal grid spacing located at the farfield boundary (Δy_∞). These grid spacings are non-dimensionalised by $\delta_{99}(x_m)$ and also the viscous length scale at the mid-point of the domain of interest, $l^+(x_m) \equiv \nu/u_\tau(x_m)$, where $u_\tau \equiv \sqrt{\tau_w/\rho}$ is the friction velocity, and τ_w the mean shear stress at the wall. In both simulations the Courant number is set to unity. The APG one-point statistics were accumulated over $884\delta_1(x_m)/U_e(x_m)$ eddy-turnover times. The ZPG one-point statistics were accumulated over $602\delta_1(x_m)/U_e(x_m)$ eddy-turnover times, and serve mainly as a point of comparison to the APG results.

2.3. Flow characterisation

The streamwise domain of interest (DoI) in the present study is from $x = 2000\delta_1(x_0)$ to $x = 3000\delta_1(x_0)$, as this range is shown to be self-similar for the APG case in section 3. As outlined in table 1, this streamwise domain corresponds to a Reynolds number range of $Re_{\delta_2} = 2500$ to 3300 for the ZPG TBL, and from $Re_{\delta_2} = 3500$ to 4800 for the APG TBL. The streamwise extent of this domain ($L_{DoI} = 1000\delta_1(x_0)$) is equivalent to 20 local boundary layer heights ($\delta_{99}(x_m)$) for the ZPG and 13 for the APG TBL, again as outlined in table 1.

The ZPG and APG boundary layer properties are now characterised within this domain of interest. We first compare the integral length scales of the two boundary layers. The displacement (δ_1) and momentum thicknesses (δ_2), as defined in (2) and (3) respectively, are illustrated in Fig. 2(a). Both of these length scales are larger in the APG TBL compared to the ZPG TBL, indicating that the boundary layer in the APG flow expands in the streamwise direction more rapidly than the ZPG case. The shape factor $H = \delta_1/\delta_2$ is illustrated in

Fig. 2(b), and changes by less than 2% over the domain of interest. The APG TBL is decelerated via the BC as illustrated in Fig. 2(c), where the maximum velocity along the profile (U_e) decreases with x. The expansion of the boundary layer coincides with a reduction of the mean wall shear stress (τ_w). In Fig. 2(d), τ_w of the APG case is less than that of ZPG TBL, as the former further expands as a result of the pressure gradient, thus reducing the mean gradient at the wall. The effect of the boundary layer expansion is also evident in the reduced skin friction coefficient ($C_f = 2\tau_w/U_e^2$) illustrated in Fig. 2(e), which is the wall shear stress nondimensionalised by the local reference velocity. The non-dimensionalised pressure gradient parameter, $\beta = \delta_1(\partial_x P_e)/\tau_w$, quantifies the strength of the pressure gradient relative to the wall shear stress, and is illustrated in Fig. 2(f). The farfield pressure gradient, $\partial_x P_e$, is evaluated at δ, and is largely independent of y for $y \geq \delta$. The parameter β is nominally 1 with a variability of $\pm 2\%$ of this value over the domain of interest.

3. Conditions for self-similarity

In this section we derive the conditions for self-similarity, and evaluate these conditions for the APG and ZPG TBL DNS. To achieve a self-similar boundary layer there are various quantities that must be independent of x. These quantities are derived from first principles following the ideas and analysis of [2, 4, 11], which are then evaluated for the present data. We start with the Reynolds averaged Navier-Stokes continuity and streamwise momentum equations specific for boundary layers given by

$$\partial_x \langle U \rangle + \partial_y \langle V \rangle = 0 \text{ , and} \tag{5}$$

$$\begin{aligned} \langle U \rangle \partial_x \langle U \rangle + \langle V \rangle \partial_y \langle U \rangle &= U_e \partial_x U_e \\ &+ \partial_x \langle vv \rangle - \partial_x \langle uu \rangle - \partial_y \langle uv \rangle + \nu \partial_y \partial_y \langle U \rangle \ , \end{aligned} \tag{6}$$

respectively, where the farfield pressure gradient has been replaced using the Bernoulli equality $\partial_x P_e = -\rho U_e \partial_x U_e$. A derivation of these equations from the complete instantaneous Navier-Stokes can be found in [40]. The following

general scaling for the mean field and Reynolds stresses is adopted with

$$\begin{aligned}
\langle U\rangle(x,y) &= U_e(x) + U_0(x)\ f(\zeta)\ , && (7)\\
\langle uv\rangle(x,y) &= -R_{uv}(x)\ r_{uv}(\zeta)\ , && (8)\\
\langle uu\rangle(x,y) &= R_{uu}(x)\ r_{uu}(\zeta)\ , && (9)\\
\langle vv\rangle(x,y) &= R_{vv}(x)\ r_{vv}(\zeta)\ \text{, and} && (10)\\
\zeta &= y/L_0(x)\ \text{, where} && (11)\\
L_0(x) &\equiv \delta_1(x)U_e(x)/U_0(x)\ . && (12)
\end{aligned}$$

The velocity scale, U_0, is used to nondimensionalise the velocity deficit. Recall U_e is the maximum velocity along the profile, and δ_1 is the displacement thickness. By substituting (7) into (2), one can then show that L_0 is defined in (12) such that

$$\int_0^{\delta/L_0} f(\zeta)\ d\zeta = -1\ . \qquad (13)$$

Likewise the integrals from $\zeta = 0$ to $\zeta = \delta/L_0$ of the similarity functions for the Reynolds stresses $r_{uv}(\zeta)$, $r_{uu}(\zeta)$ and $r_{vv}(\zeta)$ are all defined to be equal to 1. This means the functions $R_{uv}(x)$, $R_{uu}(x)$, and $R_{vv}(x)$ can be determined at each x position from the integrals in the ζ direction of $-\langle uv\rangle(x,y)$, $\langle uu\rangle(x,y)$ and $\langle vv\rangle(x,y)$, respectively.

Substituting (7) into the continuity equation (5), applying the chain rule and integration by parts, we get the following expression for the mean wall normal velocity

$$\begin{aligned}
\langle V\rangle(x,y) &= -\zeta L_0\partial_x U_e - F\partial_x\left(U_0L_0\right) + f\zeta U_0\partial_x L_0\ \text{, with} && (14)\\
F(\zeta) &= \int_0^{\zeta} f(\tilde{\zeta})\ d\tilde{\zeta}\ . && (15)
\end{aligned}$$

By substituting (7) to (10) into the momentum equation (6), along with (14) for $\langle V\rangle$, and grouping like terms produces

$$\begin{aligned}
\left[U_0\partial_x U_0\right] f^2 \quad &+ \quad \left[U_0\partial_x U_e + U_e\partial_x U_0\right] f\\
&- \quad \left[U_0U_e/L_1 + U_0\partial_x U_e\right]\zeta f' - \left[U_0^2/L_1 + U_0\partial_x U_0\right] F f'
\end{aligned}$$

$$
\begin{aligned}
&= -\left[R_{vv}/L_1\right] r'_{vv}\zeta + \left[R_{uu}/L_1\right] r'_{uu}\zeta + \left[R_{uv}/L_0\right] r'_{uv} \\
&+ \left[\partial_x R_{vv}\right] r_{vv} - \left[\partial_x R_{uu}\right] r_{uu} + \left[\nu U_0/L_0^2\right] f'' \ , \qquad (16)
\end{aligned}
$$

where $L_1 = L_0^{-1}\partial_x L_0$, and the superscript $'$ denotes $\partial/\partial\zeta$. The terms in the square brackets in (16) are only a function of x, and the remaining terms are only functions of ζ.

For a boundary layer to be self-similar each of the terms in the square brackets of (16) must have the same proportionality with x. By inspection, the first three terms in (16) imply that $U_0\partial_x U_0 \propto U_0\partial_x U_e \propto U_e\partial_x U_0$, which can only be satisfied if

$$
U_0 = KU_e \ , \qquad (17)
$$

where K is an arbitrary constant. This simplifies the definition of the length scale in (12) to $L_0 = \delta_1 U_e/U_0 = \delta_1/K$. Substituting in these relationships for U_e and L_0 into (16) and dividing through by $-U_0^2\ (\partial_x\delta_1)/\delta_1$ produces

$$
\begin{aligned}
\frac{2}{K}\Lambda f &+ \Lambda f^2 - \frac{1}{K}\left[\Lambda - 1\right]\zeta f' - \left[\Lambda - 1\right] F f' = C_{vv} r'_{vv}\zeta - C_{uu} r'_{uu}\zeta - KC_{uv} r'_{uv} \\
&- D_{vv} r_{vv} + D_{uu} r_{uu} - K^2 C_\nu f'' \ , \text{ where} \qquad (18) \\
C_{uu} &= R_{uu}/U_0^2 \ , \qquad (19) \\
C_{vv} &= R_{vv}/U_0^2 \ , \qquad (20) \\
C_{uv} &= R_{uv}/\left(U_0^2\partial_x\delta_1\right) \ , \qquad (21) \\
D_{uu} &= \partial_x R_{uu}\delta_1/\left(U_0^2\partial_x\delta_1\right) \ , \qquad (22) \\
D_{vv} &= \partial_x R_{vv}\delta_1/\left(U_0^2\partial_x\delta_1\right) \ , \qquad (23) \\
C_\nu &= -\nu/\left(U_0\delta_1\partial_x\delta_1\right) \ , \text{ and} \qquad (24) \\
\Lambda &= -\delta_1 U_0\partial_x U_0/\left(U_0^2\partial_x\delta_1\right) = -\delta_1 U_e\partial_x U_e/\left(U_e^2\partial_x\delta_1\right) \\
&= \delta_1\partial_x P_e/\left(\rho U_e^2\partial_x\delta_1\right) = \left(U_p/U_e\right)^2/(\partial_x\delta_1) \ , \qquad (25)
\end{aligned}
$$

are constants independent of x for self-similar TBL. The pressure velocity $U_p = \sqrt{(\partial_x P_e)\delta_1/\rho}$ [3], and Λ is as defined in [11]. The above scaling is derived specifically for self-similar TBL. An alternate scaling was derived in [14] derived

with application to non-self-similar flows, which can be recovered from the above analysis if one sets $K = \delta_1/\delta$ [41].

It can also be shown that if Λ, C_{uu} and C_{vv} are independent of x, then D_{uu} and D_{vv} must also be independent of x. There are, therefore, only five unique coefficients that need to be independent of x to ensure self-similarity, which are Λ, C_{uv}, C_{uu}, C_{vv} and C_ν. The Λ parameter quantifies the self-similarity of the pressure gradient term, which has already been demonstrated via the related β parameter in Fig. 2(f). The remaining coefficients are evaluated for the APG and ZPG cases.

The C_{uu} coefficients are illustrated in Fig. 3(a), and are found to be relatively constant over the domain of interest, which indicates that the profiles of $\langle uu \rangle$ are self-similar. Likewise the constant C_{vv} coefficients illustrated in Fig. 3(b) indicates that the $\langle vv \rangle$ collapse, and the constant C_{uv} coefficients in Fig. 3(c) indicate that the $\langle uv \rangle$ profiles also collapse. In fact the only term that is a strong function of x is C_ν, which measures the self-similarity of the viscous term. The C_ν coefficient of the APG case is a weaker function of x as compared to that of the ZPG TBL. How well the statistical profiles at different streamwise positions collapse will be demonstrated in the following section.

4. Scaling of the statistical profiles

Mean streamwise velocity deficit profiles ($U_e - \langle U \rangle$) are now presented at the streamwise locations indicated by the arrows in Fig. 3(a). In Fig. 4(a) the deficit profiles are non-dimensionalised by the friction velocity (u_τ) and plotted against y/δ_{99} as per the scaling adopted in [24]. The dots in this figure represent results from the previous ZPG DNS of [42], which agree with the present ZPG simulation. When scaled by u_τ, the non-dimensional velocity deficit profiles near the wall increase in the downstream direction - indicated by the arrow - as u_τ decreases. In Fig. 4(b) the profiles are illustrated scaled by U_e and δ_1, in line with the theory in the previous section. The dashed black line in the latter figures represents the streamwise average in scaled coordinates.

As undertaken for the mean velocity deficit profiles, the Reynolds stresses are now presented scaled on the basis of initially the wall shear stress and then on the basis of the outer flow (or effectively the pressure gradient). Under the former scaling the Reynolds stress profiles are nondimensionalised using a velocity scale of u_τ and the viscous length scale of ν/u_τ. Under the latter scaling the pertinent velocity and length scales are again U_e and δ_1, respectively. Profiles of $\langle uu \rangle$ are plotted in viscous scaling in Fig. 5(a), which again increase as u_τ decreases in the downstream direction. A second outer peak is also evident. Similar observations are also made concerning $\langle vv \rangle$, $\langle ww \rangle$, and $\langle uv \rangle$, plotted under viscous scaling in Fig. 5(c), Fig. 6(a), and Fig. 6(c) respectively. All of these Reynolds stresses increase in magnitude as u_τ decreases in the downstream direction, with a prominent second outer peak located between $y = \delta_1$ and $y = 1.2\delta_1$. The profiles collapse for all of the streamwise stations when plotted in outer scaling as illustrated for $\langle uu \rangle$, $\langle vv \rangle$, $\langle ww \rangle$ and $\langle uv \rangle$ in Fig. 5(b), Fig. 5(d), Fig. 6(b), and Fig. 6(d) respectively.

In summary, despite C_ν not being strictly constant throughout the domain, the mean velocity and Reynolds stresses profiles exhibit good collapse in outer scaling. This is because as the adverse pressure gradient increases, the dominant source of shear shifts from being the shear imparted by the wall, to the shear being imparted by the far field pressure gradient. The wall normal domain in which the wall shear stress (and hence C_f) is significant decreases with increasing APG.

The kinetic energy budget in the APG and ZPG TBL are also compared, but only in outer scaling. For flows in statistical steady state (i.e. time derivatives are zero) the kinetic energy budget is given by

$$0 = \mathcal{M} + \mathcal{Z} + \mathcal{T} + \mathcal{P} + \mathcal{D} + \mathcal{V} \ , \tag{26}$$

where $\mathcal{M}$ is the mean convection, $\mathcal{Z}$ pressure transport, $\mathcal{T}$ turbulent transport, $\mathcal{P}$ production, $\mathcal{D}$ is the pseudo-dissipation, and $\mathcal{V}$ the viscous diffusion. Each of these terms are defined as

$$\mathcal{M} = -\langle U_j \rangle \partial_{x_j} E \ , \tag{27}$$

$$\mathcal{Z} = -\partial_{x_i}\langle p u_i\rangle/\rho \ , \tag{28}$$

$$\mathcal{T} = -\partial_{x_j}\langle u_i u_i u_j\rangle/2, \tag{29}$$

$$\mathcal{P} = -\langle u_i u_j\rangle \ \partial_{x_j}\langle U_i\rangle \ , \tag{30}$$

$$\mathcal{D} = -\nu \left\langle (\partial_{x_j} u_i) \ (\partial_{x_j} u_i)\right\rangle \ \text{, and} \tag{31}$$

$$\mathcal{V} = = \nu \partial_{x_j}\partial_{x_j} E \ \text{, where} \tag{32}$$

$$E = \langle u_k u_k\rangle/2 \ , \tag{33}$$

is the kinetic energy. As was done for the mean and Reynolds stress profiles, each of the terms in the kinetic energy budget are time and spanwise averaged, and then scaled using U_e and δ_1 as the pertinent velocity and length scale respectively. Within the domain of interest ($2000\delta_1(x_0) \leq x \leq 3000\delta_1(x_0)$) these profiles are additionally streamwise averaged in the scaled coordinates. These streamwise averaged profiles are presented in Fig. 7(a) for the ZPG TBL and Fig. 7(b) for the APG TBL. The magnitudes and characteristics of the kinetic energy budgets are similar in both cases. However, there is a clear difference in the production and dissipation terms. The APG TBL has an outer peak in production, which the ZPG TBL does not. This outer production peak in the APG case is due to the additional mean shear throughout the boundary layer as a consequence of the pressure gradient. The only source of shear in the ZPG TBL is due to the presence of the wall. The kinetic energy produced in the outer flow is also locally dissipated in the APG flow as evidenced by the presence of the outer peak in the $\mathcal{D}$ profile.

The production to dissipation ratio is important in the context of turbulence modelling, in particular for Reynolds Averaged Navier-Stokes (RANS) type models. The present APG TBL data set could be used for the evaluation of RANS models in non-zero pressure gradient environments.

5. Two-point correlations

Finally two-point correlations are calculated in the spanwise-normal plane to give an indication of the extent to which the fluctuations are correlated in

space. The two-point correlation function is defined as

$$R_{uu}(x, y; \hat{x}, \hat{y}) \quad = \quad \frac{\langle u(x, y)\ u(\hat{x}, \hat{y})\rangle}{\sqrt{\langle u^2(x, y)\rangle\ \langle u^2(\hat{x}, \hat{y})\rangle}}\ , \tag{34}$$

where $\hat{x}$ and $\hat{y}$ are the reference locations with which the correlation is made, and the averaging is done over the spanwise direction and time. There are analogous two-point correlation function definitions for R_{vv} and R_{ww}.

In the analysis to follow $\hat{x} = 2500\delta_1(x_0)$, which is in the middle of the domain of interest, and the wall normal reference position is located at $\hat{y} = \delta_1(\hat{x})$. We select this wall normal position as it is in the vicinity of the maximum fluctuations of all of the Reynolds stresses. The correlation fields for R_{uu}, R_{vv} and R_{ww} are illustrated in Fig. 8(a), Fig. 8(b) and Fig. 8(c) respectively. The R_{uu} correlation is elliptic in shape, with the major axis tilted upwards at an approximate angle of 14° to the streamwise direction. The integral in the streamwise/wall-normal plane of the correlation field for $R_{uu} > 0.07$, is 90% of the integral of the entire positive correlation field (i.e. for $R_{uu} > 0$). We use this contour level of 0.07 to describe the length of the structures in each of the following correlation fields. For R_{uu}, the correlation is greater than 0.07 to within $6\delta_1(x_m)$ in the upstream and downstream directions. The positive correlation of the R_{vv} is more tightly packed and has a correlation higher than 0.07 to within $1.5\delta_1(x_m)$ either side of the reference location, and is not tilting toward any particular direction. Note, the integral of $R_{vv} > 0.07$ represents 52% of the integrated positive correlation field. The R_{ww} field is slanting upward with an angle of approximately 26°, which is almost double that of the R_{uu} tilt angle. The correlation is greater than 0.07 to within $0.5\delta_1(x_m)$ either side of the reference location in the direction of the minor axis of the ellipse, and surrounded by negative correlation. The integral of $R_{ww} > 0.07$ represents 80% of the integrated positive correlation field. In general the streamwise extent to which there is positive correlations in the present APG flow, is shorter than in the related ZPG DNS of [43], which has a similar maximum Reynolds number of $Re_{\delta_2} = 6650$. This indicates that the eddies in ZPG flows are more elongated than those in the present APG flow, which is also consistent with the findings of a separated TBL subjected

to a stronger APG in [44]. The interested reader can find associated two-point correlation plots for ZPG TBL in [37, 43], and for and non-self-similar APG flows in [44].

6. Concluding remarks

An adverse pressure gradient turbulent boundary layer was generated via direct numerical simulation with an appropriate farfield boundary condition to generate a self-similar flow. The coefficients quantifying the extent of self-similarity are relatively constant for the adverse pressure gradient case over a momentum thickness based Reynolds number range of $Re_{\delta_2} = 3500$ to 4800, which is equivalent to a range of 13 local boundary layer thicknesses, or 56 displacement thicknesses. Within this domain, mean velocity deficit and Reynolds stress profiles collapse under outer scaling. The Reynolds stresses also exhibit a second outer peak associated with the shear distributed throughout the boundary layer as a consequence of the application of the pressure gradient. When scaled in viscous units the Reynolds stresses in the APG TBL are significantly stronger than in the ZPG flow. The turbulent kinetic energy budget profiles also illustrate a second outer peak in the production and dissipation of the APG TBL. This again indicates that the shear distributed throughout the boundary layer generates additional fluctuations further from the wall, which are locally dissipated. Finally two-point correlations of the velocity field illustrate that statistical features are shorter in the streamwise direction than comparable ZPG TBL.

Acknowledgements

The authors would like to acknowledge the research funding from the Australian Research Council, and the computational resources provided by the Australian National Computational Infrastructure, iVEC and PRACE. Julio Soria gratefully acknowledges the support of an Australian Research Council Discovery Outstanding Researcher Award fellowship.

References

[1] V. Kitsios, L. Cordier, J.-P. Bonnet, A. Ooi, J. Soria, On the coherent structures and stability properties of a leading edge separated airfoil with turbulent recirculation, J. Fluid Mech. 683 (2011) 395–416.

[2] A. Townsend, The structure of turbulent shear flow, Cambridge University Press, 1956.

[3] G. Mellor, D. Gibson, Equilibrium turbulent boundary layers, J. Fluid. Mech. 24 (1966) 225–253.

[4] W. George, L. Castillo, Boundary layers with pressure gradient: another look at the equilibrium boundary layer, in: R. e. a. So (Ed.), Near Wall Turbulence, Elsevier, NY, 1993, p. 901910.

[5] A. Perry, I. Marusic, M. Jones, On the streamwise evolution of turbulent boundary layers in arbitrary pressure gradients, J. Fluid Mech. 461 (2002) 61–91.

[6] M. J. Lighthill, Oxford Univ. Press, London, 1963, Ch. Introduction. Boundary layer theory, book title: Laminar Boundary Layers.

[7] G. Mellor, The effects of pressure gradients on turbulent flow near a smooth wall, J. Fluid. Mech. 24 (1966) 255–274.

[8] P. Durbin, S. Belcher, Scaling of adverse-pressure-gradient turbulent boundary layers, J. Fluid. Mech. 238 (1992) 699–722.

[9] A. Perry, I. Marusic, A wall-wake model for the turbulence structure of boundary layers. Part 1. Extension of the attached eddy hpothesis, J. Fluid Mech. 298 (1995) 361–388.

[10] I. Marusic, A. Perry, A wall-wake model for the turbulence structure of boundary layers. Part 2. Further experimental support, J. Fluid Mech. 298 (1995) 389–407.

[11] L. Castillo, X. Wang, Similariy analysis for nonequilibrium turbulent boundary layers, J. Fluids Eng. 126 (2004) 827–834.

[12] A. Townsend, The development of turbulent boundary layers with negligible wall stress, J. Fluid. Mech. 8 (1960) 143–155.

[13] T. Chawla, H. Tennekes, Turbulent boundary layers with negligible wall stress: a singular-perturbation theory, Int. J. Engng Sci. 11 (1973) 45–64.

[14] M. V. Zagarola, A. J. Smits, Mean-flow scaling of turbulent pipe flow, J. Fluid. Mech. 373 (1998) 3379.

[15] T. Nickels, Inner scaling for wall-bounded flows subjecct to large pressure gradients, J. Fluid. Mech. 521 (2004) 217–239.

[16] Y. Maciel, K.-S. Rossignol, J. Lemay, Self-similarity in the outer region of adverse-pressure-gradient, AIAA J. 44 (2006) 2450–2464.

[17] R. Simpson, J. Strickland, P. Barr, Features of a separating turbulent boundary layer in the vicinity of separation, J. Fluid Mech. 79 (1977) 553–94.

[18] A. Cutler, J. Johnston, The relaxation of a turbulent boundary layer in an adverse pressure gradient, J. Fluid. Mech. 200 (1989) 367–387.

[19] K. Elsberry, F. Loeffler, M. Zhou, I. Wygnanski, An experimental study of a boundary layer that is maintained on the verge of separation, J. Fluid Mech. 423 (2000) 227–261.

[20] C. Aubertine, J. Eaton, Turbulence development in a non-equilibrium turbulent boundary layer with mild adverse pressure gradient, J. Fluid. Mech. 532 (2005) 345–364.

[21] J. Monty, Z. Harun, I. Marusic, A parametric study of adverse pressure gradient turbulent boundary layers, Int. J.Heat Fluid Flow 32 (2011) 575–585.

[22] S. Rahgozar, Y. Maciel, Low- and high-speed structures in the outer region of an adverse pressure gradient turbulent boundary layer, Exp. Thermal Fluid Sci. 35 (2011) 1575–1587.

[23] B. Stratford, An experimental flow with zero skin friction throughout its region of pressure rise, J. Fluid Mech. 8 (1959) 143–155.

[24] P. Skåre, P.-A. Krogstad, A turbulent equilibrium boundary layer near separation, J. Fluid. Mech. 272 (1994) 319–348.

[25] C. Atkinson, A.-J. Buchner, V. Kitsios, J. Soria, Experimental measurements of an equilibrium adverse pressure gradient turbulent boundary layer, in: Third symposium on fluid-structure-sound interaction and control, 2015.

[26] P. Spalart, J. Watmuff, Experimental and numerical study of a turbulent boundary layer with pressure gradients, J. Fluid. Mech. 249 (1993) 337–371.

[27] Y. Na, P. Moin, Direct numerical simulation of a separated turbulent boundary layer, J. Fluid Mech. 374 (1998) 379–405.

[28] M. Skote, D. Henningson, Direct numerical simulaiton of a separated turbulent boundary layer, J. Fluid Mech. 471 (2002) 107–136.

[29] A. Gungor, M. Simens, J. Jiménez, Direct numerical simulation of wake-perturbed separated boundary layers, J. Turb 134 (2012) 061024.

[30] M. Skote, D. Henningson, R. Henkes, Direct numerical simulation of self-similar turbulent boundary layers in adverse pressure gradients, Flow Turbulence Combust 60 (1998) 47–85.

[31] J.-H. Lee, J. Sung, Effects of an adverse pressure gradient on a turbulent boundary layer, Int. J. Heat Fluid Fl. 29 (2008) 568–578.

[32] F. Harlow, J. Welch, Numerical calculation of time-dependent viscous incompressible flow of fluid with free surface, Phys. Fluids 8 (12).

[33] J. Perot, An analysis of the fractional step method, J. Comput. Phys. 108 (1993) 51–58.

[34] S. Lele, Compact finite difference schemes with spectral-like resolution, J. Comput. Phys. 103 (1992) 16–42.

[35] M. P. Simens, J. Jiménez, S. Hoyas, Y. Mizuno, A high-resolution code for tubulent boundary layers, J. Comp. Phys. 228 (2009) 4128–4231.

[36] G. Borrell, J. Sillero, J. Jiménez, A code for direct numerical simulation of turbulent boundary layers at high reynolds numbers in BG/P supercomputers, Comp. Fluids 80 (2013) 37–43.

[37] J. Sillero, High Reynolds number turbulent boundary layers, Ph.D. thesis, Universidad Politénica de Madrid (2014).

[38] J. Sillero, J. Jiménez, R. Moser, One-point statistics for turbulent wall-bounded flows at Reynolds numbers up to $\delta^+ \approx 2000$, Phys. Fluids 25 (2013) 105102.

[39] W. Rheinboldt, Zur *a*ußeren randbedingung bei den grenzschichtgleichungen, Z. angew. Math. Mech. 36 (1956) 153–154.

[40] S. B. Pope, Turbulent flows, Cambridge University Press, 2008.

[41] C. Atkinson, V. Kitsios, A.-J. Buchner, J. Soria, Statistics and scaling of adverse pressure gradient turbulent boundary layers, in: Turbulent Shear Flow Phenomena, 2015.

[42] J. Jiménez, S. Hoyas, M. Simens, Y. Mizuno, Turbulent boundary layers and channels at moderate Reynolds numbers, J. Fluid. Mech. 657 (22) (2010) 335–360.

[43] J. Sillero, J. Jiménez, R. Moser, Two-point statistics for turbulent boundary layers and channels at Reynolds numbers up to $\delta^+ \approx 2000$, Phys. Fluids 26 (2014) 105109.

[44] A. Gungor, Y. Maciel, M. Simens, J. Soria, Analysis of a turbulent boundary layer subjected to a strong adverse pressure gradient, J. Phys. 506 (2014) 012007.

Table 1: Numerical details of the APG and ZPG TBL DNS: number of points in the streamwise (N_x), wall-normal (N_y) and spanwise (N_z) directions; domain size L_x, L_y and L_z in these respective directions non-dimensionalised by the boundary layer thickness (δ_{99}) at the inlet (x_0), and at the centre of the domain of interest ($x_m = 2500\delta_1(x_0)$); uniform streamwise (Δx) and spanwise (Δz) grid spacing and wall normal grid spacing at the wall (Δy_{wall}) and at the farfield boundary (Δy_∞) non-dimensionalised by both $\delta_{99}(x_m)$ and the viscous length scale $l^+(x_m) \equiv \nu/u_\tau(x_m)$; momentum thickness based Reynolds number (Re_{δ_2}) both across the entire domain, and within the domain of interest (DoI); streamwise extent of the domain of interest (L_{DoI}) in terms of the local $\delta_{99}(x_m)$, displacement thickness ($\delta_1(x_m)$) and momentum thickness ($\delta_2(x_m)$).

	ZPG	APG
$N_x \times N_y \times N_z$	$8193 \times 315 \times 1362$	$8193 \times 500 \times 1362$
$\left(\frac{L_x}{\delta_{99}(x_0)}, \frac{L_y}{\delta_{99}(x_0)}, \frac{L_z}{\delta_{99}(x_0)}\right)$	$(850, 40.2, 142)$	$(850, 73.5, 142)$
$\left(\frac{L_x}{\delta_{99}(x_m)}, \frac{L_y}{\delta_{99}(x_m)}, \frac{L_z}{\delta_{99}(x_m)}\right)$	$(80.4, 3.80, 13.4)$	$(54.6, 4.72, 9.12)$
$\left(\frac{\Delta x}{\delta_{99}(x_m)}, \frac{\Delta y_{\text{wall}}}{\delta_{99}(x_m)}, \frac{\Delta y_\infty}{\delta_{99}(x_m)}, \frac{\Delta z}{\delta_{99}(x_m)}\right)$	$(9.82, 0.257, 11.3, 9.82) \times 10^{-3}$	$(6.67, 0.175, 16.6, 6.67) \times 10^{-3}$
$\left(\frac{\Delta x}{l^+(x_m)}, \frac{\Delta y_{\text{wall}}}{l^+(x_m)}, \frac{\Delta y_\infty}{l^+(x_m)}, \frac{\Delta z}{l^+(x_m)}\right)$	$(10.7, 0.281, 18.2, 10.7)$	$(6.08, 0.160, 10.3, 6.08)$
Re_{δ_2} range	$300 \rightarrow 4100$	$300 \rightarrow 6100$
Re_{δ_2} range in DoI	$2500 \rightarrow 3300$	$3500 \rightarrow 4800$
$\left(\frac{L_{DoI}}{\delta_{99}(x_m)}, \frac{L_{DoI}}{\delta_1(x_m)}, \frac{L_{DoI}}{\delta_2(x_m)}\right)$	$(20, 113, 159)$	$(13, 56, 87)$

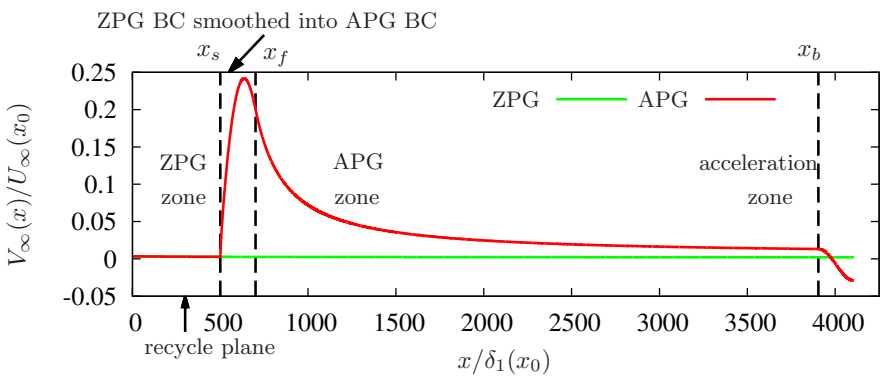

Figure 1: Farfield wall normal velocity boundary condition in the APG (red line) and ZPG (green line) DNS. The following labels refer specifically to the APG TBL DNS: x_s - position prior to which BC is governed by equation (1); x_f - position after which BC is governed by equation (4); x_b - position at which blowing into the computational domain is initiated.

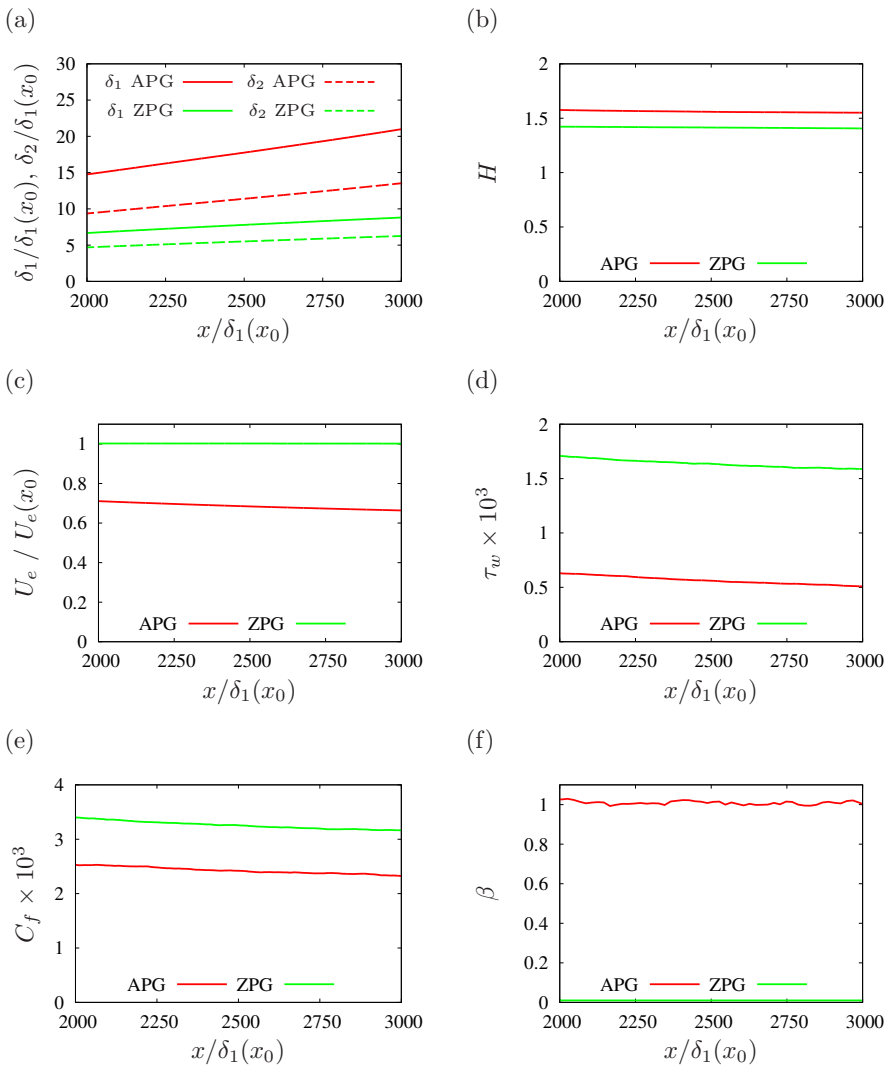

Figure 2: Boundary layer properties of the APG and ZPG DNS: (a) displacement (δ_1) and momentum (δ_2) thicknesses; (b) shape factor, $H = \delta_1/\delta_2$; (c) outer reference velocity, U_e; (d) wall shear stress, τ_w; and (e) skin friction coefficient, $C_f = 2\tau_w/U_e^2$; and (f) pressure gradient parameter, $\beta = \delta_1(\partial_x P_e)/\tau_w$.

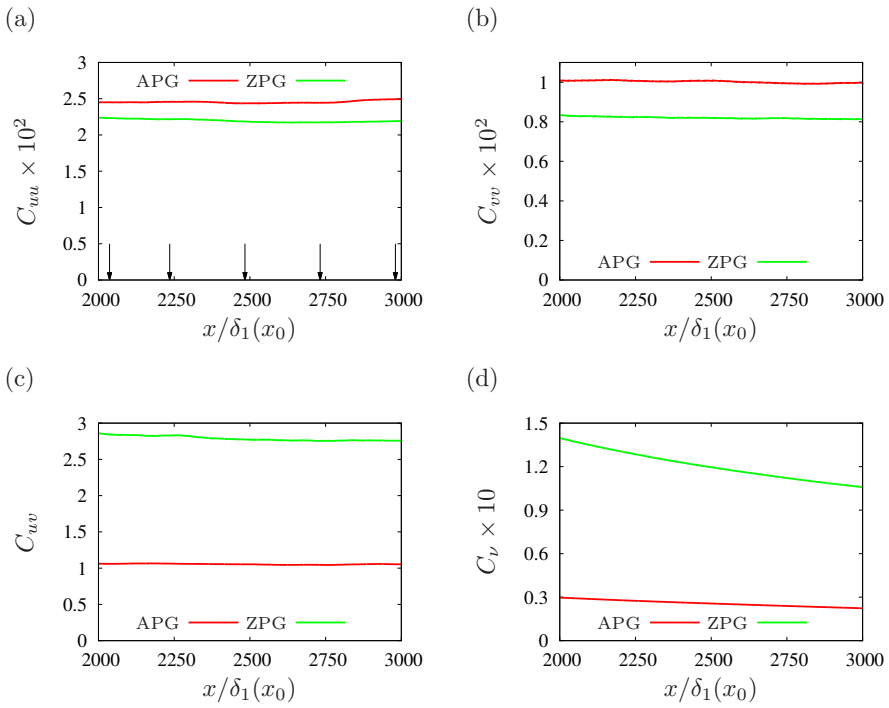

Figure 3: Coefficients to assess the self-similarity of the APG and ZPG TBL DNS on the basis of: (a) C_{uu}, with arrows indicating the positions of the APG TBL velocity profiles illustrated in Fig. 4, Fig. 5 and Fig. 6; (b) C_{vv}; (c) C_{uv};and (d) C_ν.

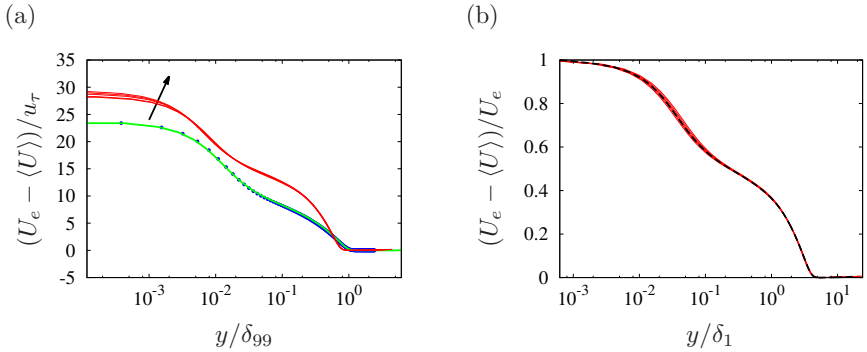

Figure 4: Mean velocity deficit profiles ($U_e - \langle U \rangle$) nondimensionalised by: (a) friction velocity, u_τ, and boundary layer thickness, δ_{99}; and (b) reference outer velocity, U_e, and displacement thickness, δ_1. ZPG TBL DNS of [42] - blue dots; ZPG TBL DNS current simulation - green line; APG TBL DNS from current simulation at different streamwise locations - red lines; streamwise averaged scaled profiles - dashed black lines. Positions of the APG TBL profiles are illustrated in Fig. 3(a), with arrows in left column indicating the direction of increasing x position.

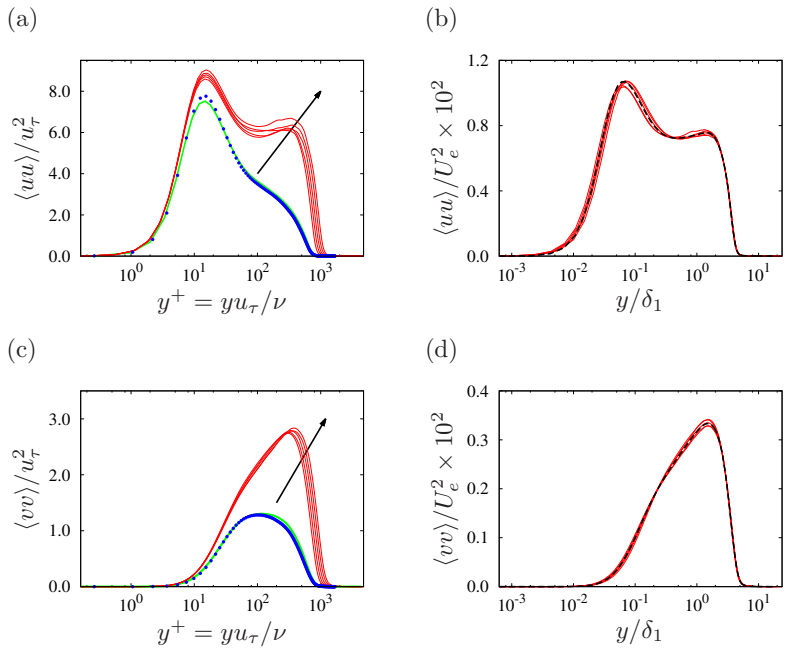

Figure 5: Reynolds stress profiles: (a) $\langle uu \rangle$ in viscous scaling nondimensionalised by friction velocity, u_τ, and viscous length scale, ν/u_τ; (b) $\langle uu \rangle$ in outer scaling nondimensionalised by reference outer velocity, U_e, and displacement thickness, δ_1; (c) $\langle vv \rangle$ in viscous scaling; (d) $\langle vv \rangle$ in outer scaling; Refer to caption of Fig. 4 for line correspondence.

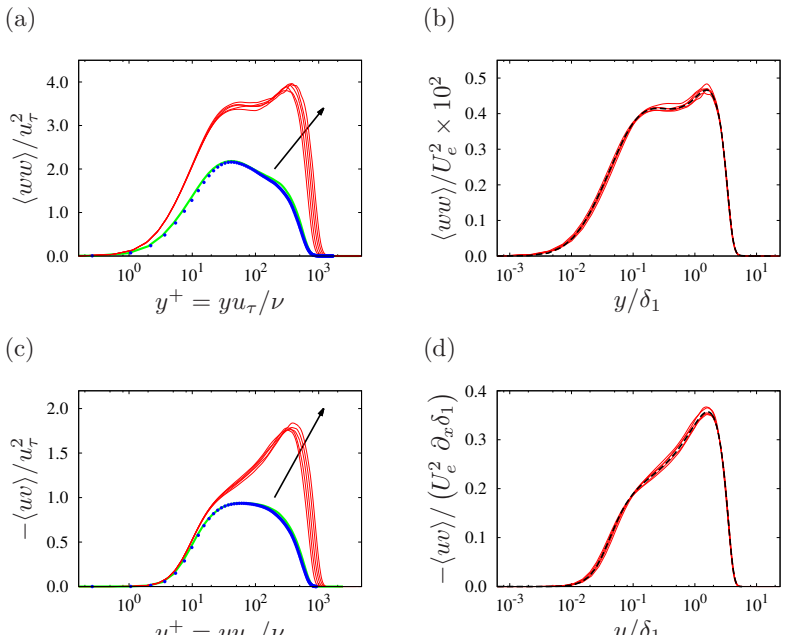

Figure 6: Reynolds stress profiles: (a) $\langle ww \rangle$ in viscous scaling; (b) $\langle ww \rangle$ in outer scaling; (c) $\langle uv \rangle$ in viscous scaling; and (d) $\langle uv \rangle$ in outer scaling. Refer to caption of Fig. 4 for line correspondence.

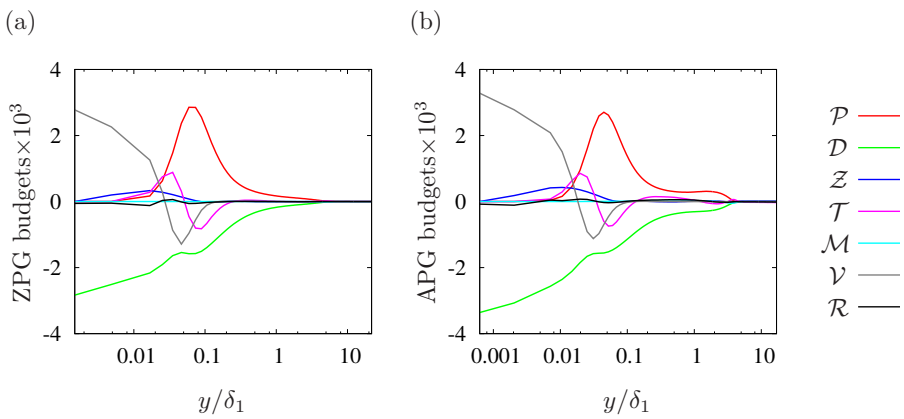

Figure 7: Streamwise averaged budget profiles nondimensionalised by U_e and δ_1 for: (a) ZPG TBL; and (b) APG TBL. The mathematical definition of the mean convection ($\mathcal{M}$), pressure transport ($\mathcal{Z}$), turbulent transport ($\mathcal{T}$), production ($\mathcal{P}$), pseudo-dissipation ($\mathcal{D}$), and viscous diffusion ($\mathcal{V}$), are all defined in equations (27) to (32) respectively. $\mathcal{R}$ is the residual given by the negative sum of all of the terms in the kinetic energy budget.

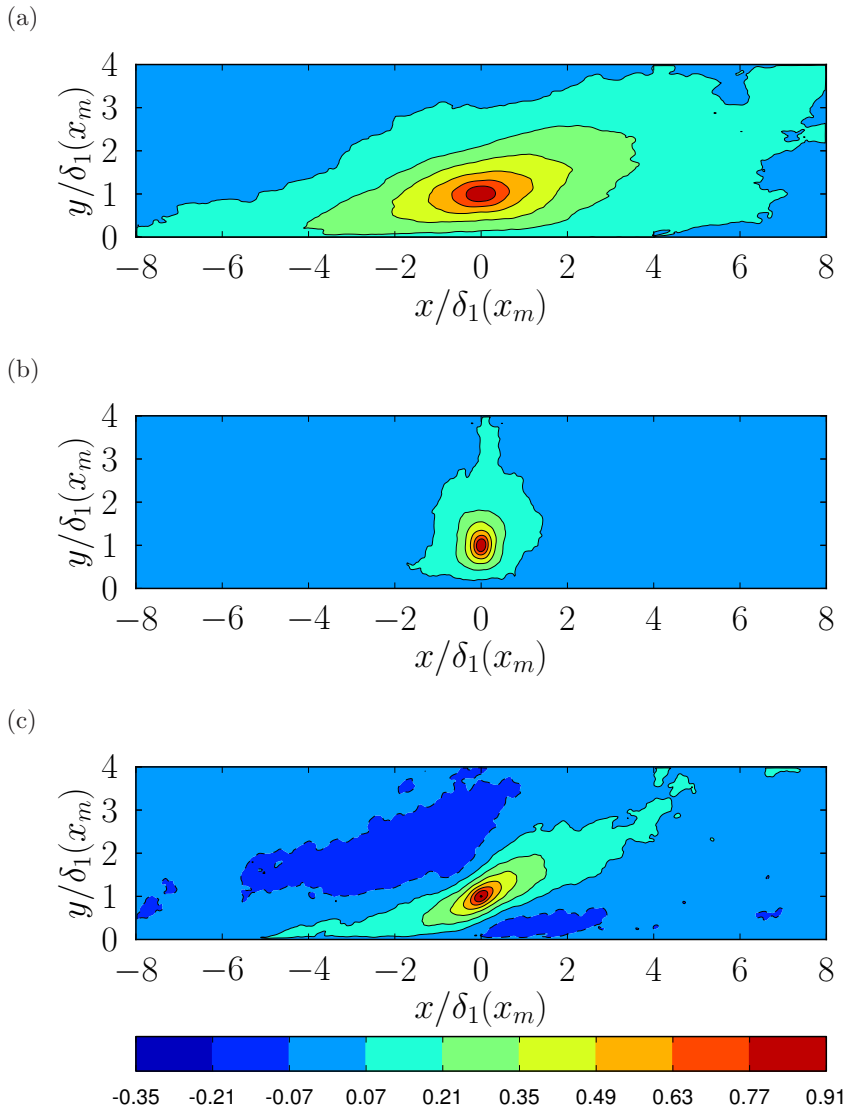

Figure 8: Two-point spatial correlation coefficients centred at $x = 5000\delta_1(x_0)$ (centre of the domain of interest) and $y = \delta_1$: (a) R_{uu}; (b) R_{vv}; and (c) R_{ww}, with the colour bar representative for all figures. The horizontal and vertical axes are to scale.